PCCP

ROYAL SOCIETY OF CHEMISTRY

PAPER

View Article Online
View Journal | View Issue

Cite this: *Phys. Chem. Chem. Phys.*, 2020, **22**, 2540

Similarities and differences between potassium and ammonium ions in liquid water: a first-principles study†

Fikret Aydin,‡[a] Cheng Zhan,‡[a] Cody Ritt,[b] Razi Epsztein,[bc] Menachem Elimelech,[b] Eric Schwegler[a] and Tuan Anh Pham*[a]

Received 14th November 2019,
Accepted 8th January 2020

DOI: 10.1039/c9cp06163k

rsc.li/pccp

Understanding ion solvation in liquid water is critical in optimizing materials for a wide variety of emerging technologies, including water desalination and purification. In this work, we report a systematic investigation and comparison of solvated K^+ and NH_4^+ using first-principles molecular dynamics simulations. Our simulations reveal a strong analogy in the solvation properties of the two ions, including the size of the solvation shell as well as the solvation strength. On the other hand, we find that the local water structure in the ion solvation is significantly different; specifically, NH_4^+ yields a smaller number of water molecules and a more ordered water structure in the first solvation shell due to the formation of hydrogen bonds between the ion and water molecules. Finally, our simulations indicate that a comparable solvation strength of the two ions is a result of an interplay between the nature of ion–water interaction and number of water molecules that can be accommodated in the ion solvation shell.

1 Introduction

Understanding solvation properties of ions in liquid water is essential for predicting and optimizing device performance for a wide variety of emerging energy and environmental technologies, including water desalination and purification.[1–5] For instance, in desalination processes involving reverse osmosis, nanofiltration, or ion-exchange membranes, water molecules surrounding an ion are partially removed during ion permeation, which contribute to the overall energy barrier associated with ion transport through the pore.[6–8] In this regard, understanding the difference in the solvation strength among ions is particularly important in determining ion selectivity.[9,10]

For the past several decades, extensive studies have been carried out to investigate properties of ions in liquid water and complex environments, such as nanopores and membranes.[11–17] In the context of ion rejection by membranes, much of the existing studies have explained the trend in selectivity based on the correlation between the activation energy for ion permeation and its hydration energy that represents the solvation strength. For instance, Epsztein *et al.*[7] and Richards *et al.*[18] showed that fluoride anion experiences the highest energy barrier for transport through polyamide membranes among halide anions, which can be attributed to a much higher hydration energy of the ion. More recently, several studies show that ion selectivity can be more complex, as it may depend not only on the hydration energy but also on the size, shape and chemical compositions of the ions. For example, recent studies show that the unique geometry of the solvation structure of nitrate is largely responsible for the ion to be electrosorbed preferentially over chloride ion in ultramicroporous carbons and ion-exchange membranes.[8,19] In this regard, a detailed understanding of how solvation properties vary across ions with different chemical composition, size and shape is critical for optimizing materials for selectivity.[20]

In this work, we present a detailed investigation and comparison of solvation properties of two common cations, K^+ and NH_4^+, in liquid water using first-principles molecular dynamics (FPMD) simulations based on density functional theory. Our study of NH_4^+ is motivated by the importance of the ion in a number of chemical and biological processes, such as protein folding in living organisms,[21,22] and in several emerging technologies, including design of synthetic receptors[23] and water treatment.[24,25] For instance, NH_4^+ removal from wastewater is of particular importance as it is a major component of the nitrogen species in wastewaters, for which a high concentration can lead to eutrophication of natural waterways.[26] Finally, from a more fundamental perspective, NH_4^+ is a relatively simple polyatomic ion that represents an ideal candidate to be compared

[a] *Lawrence Livermore National Laboratory, Livermore, California, 94551, USA. E-mail: pham16@llnl.gov*
[b] *Department of Chemical and Environmental Engineering, Yale University, New Haven, CT, 06520-8286, USA*
[c] *Faculty of Civil and Environmental Engineering, Technion-Israel Institute of Technology, Technion City, Haifa 32000, Israel*

† Electronic supplementary information (ESI) available. See DOI: 10.1039/c9cp06163k

‡ Authors with equal contribution.

to other well-studied alkali metal ions. Here, we chose to compare NH_4^+ to K^+ as these two ions are known to exhibit very similar solvation properties in liquid water despite the fact that they possess rather different chemical compositions and ionic radius.[27] Specifically, it has been reported that NH_4^+ yields a hydration energy of 285 kJ mol^{-1}, which is only about 10 kJ mol^{-1} smaller than that of K^+.[27] In this regard, we aim to elucidate the origin of the comparable hydration energy of the two ions, and to understand how the solvation strength of the ions is governed by the their chemical composition.

The remainder of the paper is organized as follows. First, we describe our computational methods, including the construction of the solution model and the details of our first-principles calculations. Then, we discuss our results regarding the comparison in the solvation strength and structures between solvated K^+ and NH_4^+, and we elucidate the origin of the comparable hydration stability of the two ions. Finally, we discuss our main conclusions.

2 Methods

All solutions were modeled by periodic cubic cells consisting of 63 water molecules and a single solvated ion, with the excess charge compensated by a uniform background charge. The size of the cells was chosen to yield the experimental density of liquid water under ambient conditions, which results in a salt concentration of 0.87 M for both solutions. Our first-principles simulations were carried out using Born–Oppenheimer MD with the Qbox code,[28] with the interatomic force derived from density functional theory (DFT) and the Perdew, Burke, and Ernzerhof (PBE) approximation for the exchange–correlation energy functional.[29] The interaction between valence electrons and ionic cores was represented by norm-conserving pseudopotentials,[30] and the electronic wave functions were expanded in a plane-wave basis set truncated at a cutoff energy of 85 Ry. All hydrogen atoms were replaced with deuterium to maximize the allowable time step, which was chosen to be 10 atomic units. The equilibration runs were carried out at an elevated temperature of $T = 400$ K in order to recover the experimental water structure and diffusion, while also providing a good description of the ion solvation at room temperature.[31–33]

The FPMD simulations were carried out at a constant temperature (*NVT* condition) using a velocity scaling thermostat. For each solution, we performed five runs in parallel, starting with different uncorrelated samples. In total, we collected over 200 ps (5×40 ps) of simulation data for each solution. For each run, the analysis was then carried out using 30 ps after 10 ps equilibration; accordingly, the results presented below for each solution were obtained using around 150 ps production simulations. We have also carried out a shorter simulation (20 ps) of NH_4^+ using a more sophisticated Bussi–Donadio–Parrinello (BDP) thermostat,[34] and we find that the change of the themostat does not affect the ion solvation structure within the statistical error of the simulation (see ESI†).

We note that, beside the PBE functional, a large number of more sophisticated approximation for the exchange–correlation functional has been recently employed for the simulation of liquid water. For instance, it has been shown that the inclusion of van der Waals (vdW) corrections to the PBE functional improves the description of structural properties of liquid water.[35–37] Similarly, the use of the PBE0 hybrid density functional that includes 25% of the non-local Hartree–Fock exchange energy leads to a better description of structural properties of water beyond that of PBE;[38] and an even better agreement with experiment was obtained when the vdW correction is combined with the PBE0 functional.[36] More recently, it was shown that the use of a dielectric-dependent hybrid (DDH) density functional with a fraction of exact exchange defined as the inverse of the high-frequency dielectric constant of liquid water leads to an excellent description of not only structural and dynamical properties but also the electronic structure of liquid water.[39] Finally, employment of the SCAN meta-GGA functional at a temperature of 330 K was also shown to provide a very good description of liquid water at ambient conditions.[40,41] In this work, our simulations were carried out using the PBE functional at an elevated temperature, as this simulation protocol has been shown to provide a reasonable description of liquid water and complex solutions, such as those with solvated ions and at heterogeneous interfaces, at a low computational cost.[31,42–50] We note that the use of more accurate functionals, such as hybrid functionals, for the long simulation times presented here would involve significant computational resources.[51–53]

In addition to the investigation of ion solvation structure using MD simulations, we also estimated ion solvation energy (ΔE_{sol}) based on cluster calculations. Specifically, ΔE_{sol} was approximated as the binding energy of the $X^+(H_2O)_n$ clusters, where $X \equiv K^+$ or NH_4^+, and n is the number of water molecules in the first ion solvation shell. In this way, the solvation energy of the ion is estimated as

$$\Delta E_{sol} = E_{X^+} + E_{(H_2O)_n} - E_{X^+(H_2O)_n}, \quad (1)$$

where $E_{X^+(H_2O)_n}$, $E_{(H_2O)_n}$, and E_{X^+} are the energies of the $X^+(H_2O)_n$ and $(H_2O)_n$ clusters, and the ion X^+ in vacuum, respectively. In these calculations, configurations of the $X^+(H_2O)_n$ clusters were extracted directly from the FPMD simulations. Specifically, the solvation energies were computed for 500 configurations of $X^+(H_2O)_n$ extracted at equal time intervals (0.3 ps) from the corresponding FPMD simulations. For each cluster, the number of water molecules, n, was determined using the distance cutoff as the first minimum of the radial distribution function between the ion and water oxygens. We note that our calculation of the ion solvation energy does not take into account the contribution of the solvation entropy, which is generally small (3–4% of the total solvation free energy for K^+).[54]

3 Results and discussion

3.1 Analogies in the ion solvation

Our initial examination of solvated K^+ and NH_4^+ is based on the analysis of radial distribution functions (RDF) between the ions and water oxygen atoms, $g_{XO}(r)$, where X is K^+ or the nitrogen atom of NH_4^+. Focusing first on K^+, we find that the first

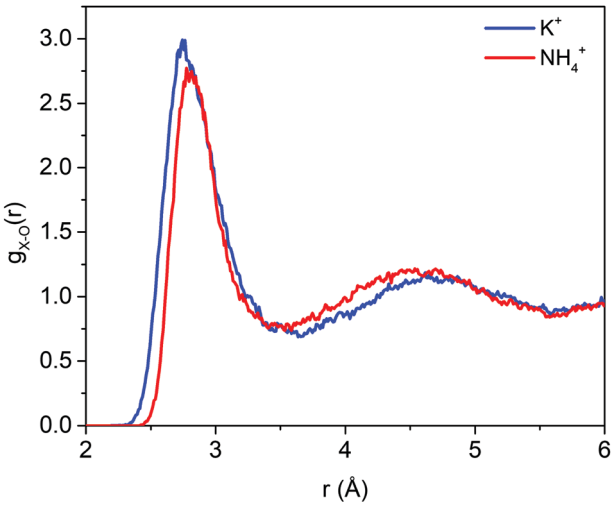

Fig. 1 Ion-oxygen radial distribution functions, $g_{XO}(r)$, for solvated K^+ and NH_4^+ in liquid water, as obtained from first-principles molecular dynamics simulations. Blue and red lines indicate results obtained for X corresponding to K^+ and nitrogen atom of NH_4^+, respectively.

maximum of $g_{KO}(r)$ shown in Fig. 1 is located at 2.77 Å, which is in good agreement with the experimental value of 2.73–2.79 Å determined by X-ray adsorption measurements.[55,56] Interestingly, we find that the experimental peak position is reproduced at a similar accuracy (within 0.02 Å) as the SCAN functional,[56] although the latter represents a more sophisticated approximation for the exchange correlation energy compared to the PBE functional that is currently employed.[57,58] While this observation indicates that our simulation protocol provides a reasonable description of the ion solvation structure, it is necessary to emphasize that nuclear quantum effects (NQEs), which are not fully included in these simulations, may play additional important role in the description of structural and dynamical properties of the ions. For instance, it has been shown that a good description of dynamical properties of liquid water obtained with the revPBE-D3 functional and a classical treatment of the nuclei was partially due to a cancellation of errors in the functional and the neglect of NQEs.[37]

Notably, when compared to K^+, Fig. 1 shows that NH_4^+ exhibits an analogous RDF, both in the peak position and intensity. For instance, the RDF obtained for NH_4^+ yields a value of 2.78 Å for the position of the first maximum, which is only within 0.1 Å compared to that of K^+. In addition, we find that the first RDF minimum of K^+ is located at 3.71 Å, which is slightly larger than that of NH_4^+ (3.54 Å). Our initial structural analysis therefore points to a distinct similarity in the size of the first solvation shell of K^+ and NH_4^+. While this conclusion leads to an impression that the two ions would yield similar solvation properties, as we discuss in more detail below, the local solvation structure surrounding K^+ and NH_4^+ can be significantly different.

3.2 Differences in the water structure in the ion solvation

In order to elucidate the difference in the local solvation structure of K^+ and NH_4^+, we calculated the number of water molecules in the first solvation shell of the ions, n_{XO}. Here, n_{XO} was obtained by integrating the corresponding RDFs to their first local minimum. We find that the number of water molecule in the ion solvation shell is smaller for NH_4^+, yielding an average value of 5.2 as compared to a corresponding result of 6.8 for K^+. The distributions of n_{XO} shown in Fig. 2a also indicate that NH_4^+ and K^+ prefer an oxygen coordination number of five and seven in the first solvation shell, respectively. These results indicate that the water structure surrounding K^+ and NH_4^+ is rather different, which is further illustrated in Fig. 2b and c, where the typical solvation structures of NH_4^+ and K^+ are presented. We note that our results for the number of water molecule in the ion solvation shell presented here are also in agreement with values of 6.0–6.1 ± 1.0[55,59] and 5.3–5.8[60,61] previously reported for K^+ and NH_4^+, respectively.

In addition to the oxygen coordination number, the difference in the water structure surrounding the ion can be obtained by examining the ion-oxygen incremental RDFs. Specifically, these incremental RDFs separate the overall RDF distribution presented in Fig. 1 into contributions from the closest water molecules. As shown in Fig. 3, despite the total ion-oxygen RDFs of NH_4^+ and K^+ are similar, we find that the incremental RDFs of the two ions are substantially different. Specifically, it is found that K^+ has five tightly bound water molecules in the first solvation shell, and that the sixth and seventh water molecules bridging the first and second hydration shells. On the other hand, the first solvation shell of NH_4^+ is formed by

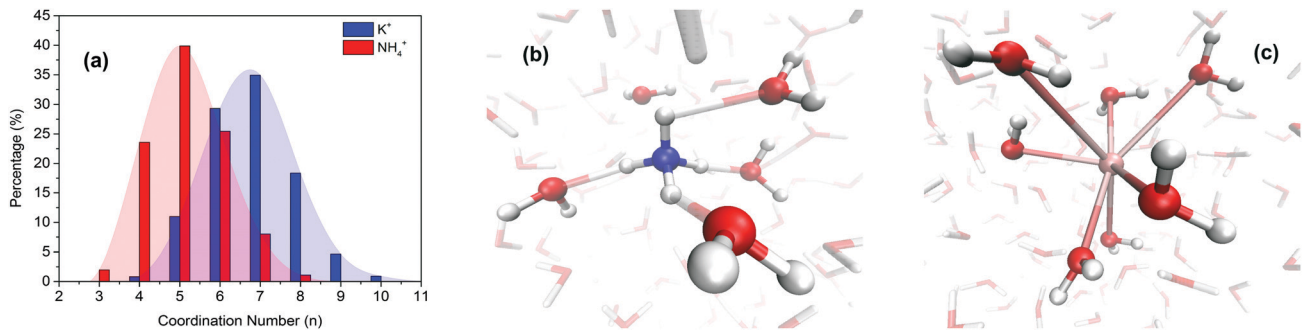

Fig. 2 (a) Histograms of the oxygen coordination number in the first solvation shell around NH_4^+ (red) and K^+ (blue) ions in liquid water. The first minima in the corresponding $g_{XO}(r)$ were used as distance cutoffs for determination of the first solvation shells. Typical solvation structures of NH_4^+ (b) and K^+ (c) with five and seven water molecules in the first shell, respectively.

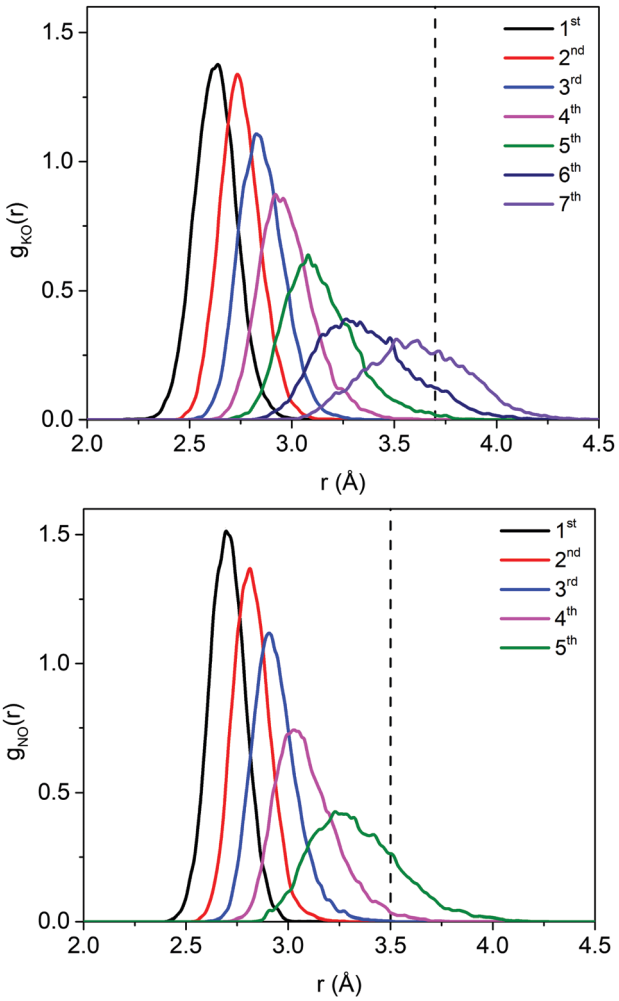

Fig. 3 Incremental ion-oxygen radial distribution functions computed for K^+ (upper panel) and NH_4^+ (lower panel) ions in liquid water. The dashed lines indicate the position of the first minimum of the corresponding total RDF shown in Fig. 1.

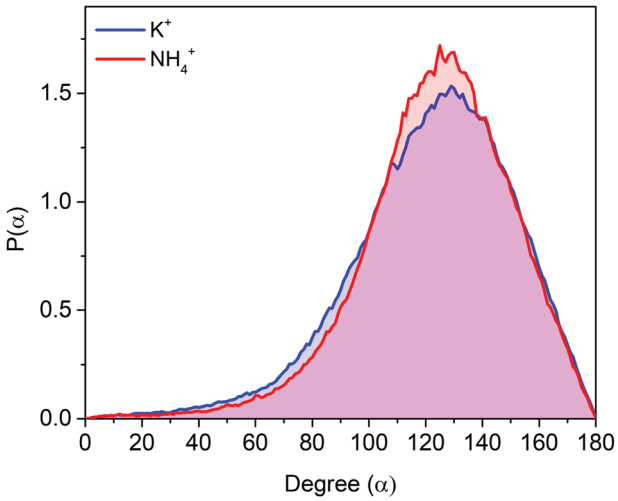

Fig. 4 Distribution $P(\alpha)$ of the tilt angle (α) between the oxygen-ion position vector and dipole moment vectors of water molecules within the first solvation shell of K^+ (blue) and NH_4^+ (red).

four tightly bound water molecules and a fifth water molecule that is exchanged between the first and second solvation shell.

Notably, Fig. 3 shows that the incremental RDFs of NH_4^+ are more tightly packed. In particular, we find that their peak positions are distributed within a narrower range of 2.7–3.3 Å as compared to the corresponding value of 2.6–3.6 Å obtained for K^+. This suggests that water molecules in the first solvation shell of NH_4^+ is generally more uniformly distributed than K^+. This conclusion is further corroborated by examining the distribution of the tilt angle between dipole moment vectors of water molecules and the vector joining the water's oxygen and the cations, shown in Fig. 4. We find that the tilt angle computed for water molecules in the first solvation shell of the two ions exhibit a similar distribution, with a peak centering around 130°. However, the NH_4^+ distribution is slightly narrower and yields a higher intensity in the main peak. In addition, the tilt angle computed for NH_4^+ yields an average value of 123.8° as compared to 119.7° obtained for K^+. Such a larger average tilt angle obtained for NH_4^+ is consistent with the analysis of incremental RDFs, indicating that water structure in the first shell of NH_4^+ is generally more ordered than that of K^+.

Next, to better understand the ordering of water molecules in the solvation shell of NH_4^+, we investigated in more detail the RDF between hydrogen atoms of the ion and water oxygens. As shown in Fig. 5a, we find that the coordination number of each hydrogen of NH_4^+ is 1.0, as obtained by integrating the RDF up to the first minimum. This indicates that the four water molecules that reside within the first solvation shell are hydrogen bonded with the hydrogen atoms of ammonium, and together form a distinct tetrahedral cage around the ion, as clearly shown in the spatial distribution function of oxygen around the ion shown in Fig. 5b. We also find that the fifth water molecule that bridges the first and second solvation shells of the ion is more mobile, and tends to occupy the center of the tetrahedral faces defined by the other four water molecules. Overall, our analysis indicates that the ordering of water structure near NH_4^+ is related to the formation of hydrogen bonds with the ion, consistent with results reported in previous first-principles studies.[60,62]

Our simulations therefore indicate that although K^+ and NH_4^+ exhibit a similar size of the ion solvation shell, the local water structure around the two ions is rather different. More specifically, it is shown that NH_4^+ yields a smaller number of water molecules in the first solvation shell, and these water molecules exhibit more ordered structure compared to those of K^+ due to the formation of hydrogen bonds with hydrogen atoms of NH_4^+.

3.3 Strength of the ion solvation

We now turn to discuss the solvation strength of the two ions, which is directly related to their hydration energy. This quantity is particularly important as it defines the ion solvation structure as well as the energetics and kinetics of ion selectivity.[20] Histogram of the solvation energy computed using eqn (1) is shown in Fig. 6 for K^+ and NH_4^+. We find that the two ions exhibit a very similar distribution; nevertheless, a closer investigation shows that the

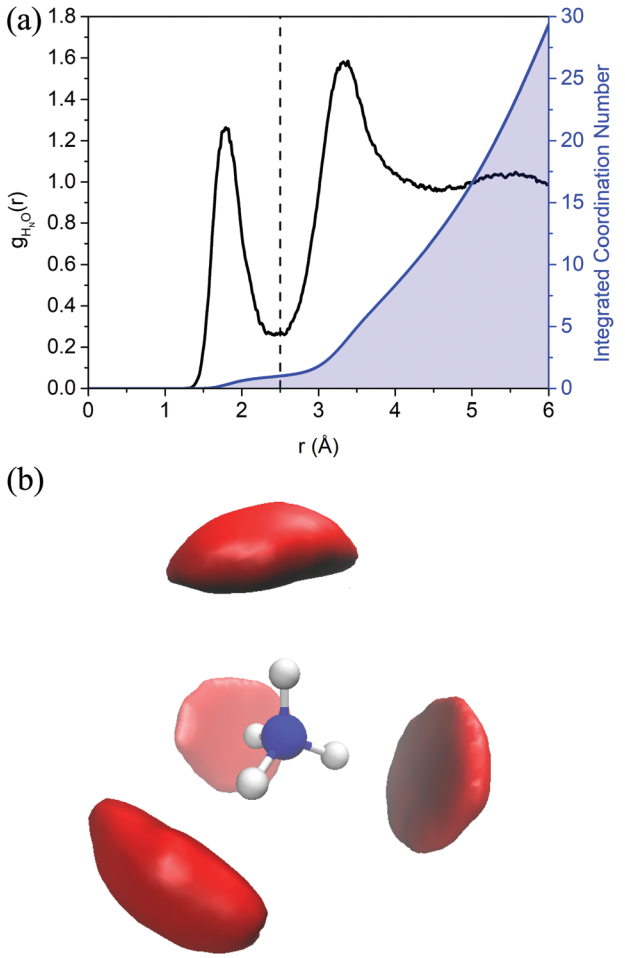

Fig. 5 (a) Radial distribution function computed for water oxygen and hydrogen of NH_4^+ (black), and the corresponding integrated oxygen coordination number (blue); (b) spatial distribution function of water oxygen around the cation.

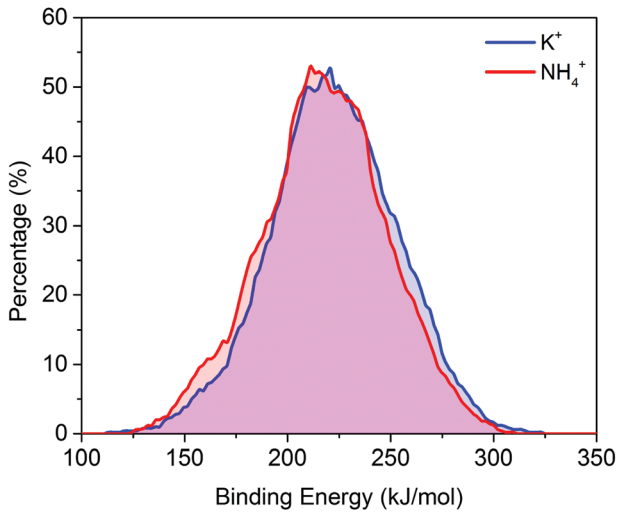

Fig. 6 Distribution of the solvation energy (ΔE_{sol}) estimated from the binding energy of the $X^+(H_2O)_n$ clusters, where n is the number of water molecules in the first ion solvation shell, and $X \equiv K^+$ (blue) or NH_4^+ (red). The results were obtained for 500 structural configurations extracted at equal time intervals from first-principles simulations of each solution.

average binding energy of NH_4^+–water clusters is slightly smaller by about 4.7 kJ mol^{-1} when compared to that of K^+–water ones. This conclusion is in line with existing experimental data, where it was shown that the hydration energy of NH_4^+ is only about 10 kJ mol^{-1} smaller than that of K^+. It is also important to point out that K^+ yields an average value of ΔE_{sol} = 239.4 kJ mol^{-1} at the PBE level of theory, which is in reasonable agreement with the experimental value of 295 kJ mol^{-1} for the hydration energy of the ion.[63] Our results therefore indicate that the ion hydration energy is largely determined by the interactions between the ion and water molecules that constitute the first ion solvation shell, and that cluster calculations employed here provide a reasonable estimate for the hydration energy of the ions.

Collectively, our results show that, although K^+ and NH_4^+ exhibit distinct differences in the neighbouring water structure, they yield a rather similar solvation strength. Interestingly, we find that NH_4^+ yields a slightly weaker solvation energy compared to K^+ although it yields a more ordered water structure in the first solvation shell. This, however, contradicts the common behavior of simple monovalent ions, such as halide and alkali metal ions in liquid water, where it is known that the ions that exhibit a more ordered water structure also possess a stronger hydration energy.[64,65] As we discuss below, a comparable solvation strength of K^+ and NH_4^+ stems from a complex interplay between several factors, including the nature of the ion–water interaction, and the number of water molecules that can be accommodated in the ion solvation shell.

3.4 The role of ion–water interaction

In order to understand the origin of a more ordered water structure in the first solvation shell of NH_4^+, as well as the solvation strength of NH_4^+ and K^+, it is instructive to investigate in more detail the ion–water interaction of the two ions. To this end, we computed and compared the binding energy of the ions with the same number of water molecules. Specifically, this is obtained by considering ion–water cluster containing a single water molecule, as well as five and seven water molecules. The latter scenarios represent preferred water coordination numbers in the first solvation shell of NH_4^+ and K^+.

We find that, for the system consisting of a cation and a single water molecule, NH_4^+ yields a stronger binding energy with the water molecule by about 22.4 kJ mol^{-1} than K^+. Moving to more complex ion–water clusters, we report in Fig. 7a and b histograms of the ion–water binding energies computed for clusters with five and seven water molecules, respectively. Here, similar to the calculation of ΔE_{sol} discussed above, the binding energies were obtained using 500 configurations extracted from the corresponding FPMD simulations. We find that for the same number of water molecules, the ion–water binding energy is always larger for NH_4^+. Specifically, for the ion–water cluster containing five water molecules, the binding energy computed for NH_4^+ is stronger than that of K^+ by 18.4 kJ mol^{-1} at the PBE level of theory. This difference is reduced for the larger clusters with seven water molecules; however the ordering in the

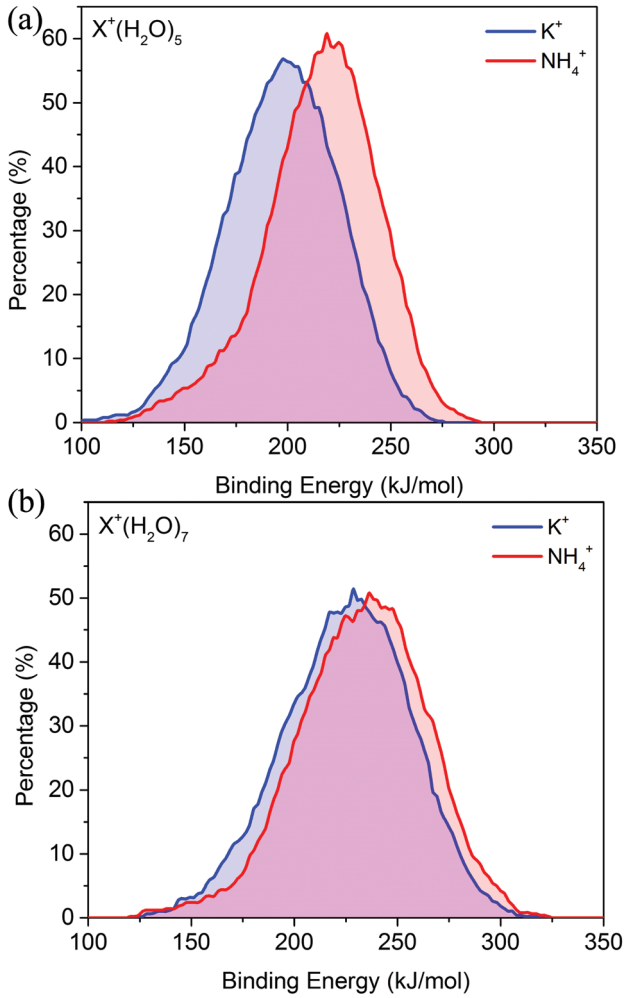

Fig. 7 Distribution of the binding energy of $X^+(H_2O)_n$ clusters, where n is the number of water molecules in the first ion solvation shell, and $X \equiv K^+$ (blue) or NH_4^+ (red). The results obtained for clusters with five and seven water molecules are shown on the upper and lower panels, respectively.

solvation energy remains, with the binding energy of the NH_4^+ cluster is about 7.3 kJ mol^{-1} larger. This observation indicates that the ion–water interaction is generally stronger for NH_4^+, which explain for a more ordered water structure in the first solvation shell of the ion compared to K^+.

Although the conclusion of a stronger ion–water interaction for NH_4^+ is consistent with the fact that the ion yields a more ordered water structure in the first solvation shell, this does not explain why NH_4^+ has a slightly overall weaker solvation energy ΔE_{sol} compared to K^+ as discussed above. For the latter, a possible explanation is related to a larger number of water molecules involved in the first solvation shell of K^+ (6.8) compared to NH_4^+ (5.2), which in turn introduces additional ion–water interaction that stabilize the ion solvation of K^+. This is indeed supported by our calculations, where we find that the binding energy computed for K^+ clusters with seven water molecules is stronger by 9.38 kJ mol^{-1} than that computed for NH_4^+ clusters with five water molecules. We emphasize again that five and seven water molecules correspond to the preferred coordination numbers in the first solvation shell of NH_4^+ and K^+, respectively.

Our simulations therefore indicate that the overall solvation strength of the ion is not only determined by the ion–water interaction, but also by the number of water molecules in the shell. In particular, K^+ can accommodate a larger number of water molecules, which leads to an overall slightly stronger ion solvation strength compared to NH_4^+. On the other hand, even though NH_4^+ appears to interact more strongly with individual water molecules, the overall solvation strength is slightly weaker due to its unique chemical composition that limits the total number of water molecules in the solvation shell. More specifically, the presence of four hydrogen atoms that can form relatively stable hydrogen bond with surrounding water is responsible for a smaller number of water molecules in the solvation shell of NH_4^+.

Finally, we briefly discuss existing studies of solvated ions using continuum models, and how they are related to the current findings. Recent studies using coarse-grained lattice Monte Carlo simulations and Ginzburg–Landau (GL) theory have pointed to the saturation of water dipole moment in the first ion solvation shell, while indicating that this effect plays a dominant role in determining the solvation free energy of solvated ions.[66,67] Along this direction, it has also been shown that the GL theory successfully reproduces the solvation energy of various ions in liquid water and other solvents.[68] Our study provides several evidences that support these continuum models. Specifically, our simulations point to ordered water structure around K^+ and NH_4^+, which resembles the saturation of water dipole moment near the ions discussed in previous studies.[66–68] In addition, we find that ion solvation energy is largely determined by ion interactions with water molecules in the first ion solvation shell, also consistent with the conclusion that saturation of water dipole moment plays a dominant role in determining the solvation energy. Last but not least, in line with these existing continuum models, our first-principles simulations point to the importance of solvent reorganization and dielectric inhomogeneity in the description of solvated ions.[69]

4 Conclusions

We investigated the solvation properties of K^+ and NH_4^+ in liquid water using first-principles molecular dynamics simulations based on density functional theory. Our simulations reveal strong similarities in the overall solvation of the two ions. In particular, we find that the two ions exhibit a similar size in the solvation shell as well as solvation strength. On the other hand, we find that the local water structure in the ion solvation is significantly different. Specifically, it is shown that NH_4^+ yields a smaller number of water molecules in the first solvation shell, *i.e.*, 5.2 compared to a value of 6.8 for K^+. In addition, our analysis shows that water molecules in the solvation shell of NH_4^+ exhibit more ordered structure compared to those of K^+ due to the formation of hydrogen bonds with hydrogen atoms of NH_4^+.

Our simulations point to a complex interplay between the nature of ion–water interactions and the number of water molecules in the solvation shell on the strength of ion solvation in liquid water. Specifically, we show that the larger NH_4^+ ion yields a slightly weaker solvation energy than K^+ by about 4.7 kJ mol^{-1}, despite exhibiting a stronger interaction with individual water molecules. We find that this counterintuitive behavior is related to the unique chemical composition of NH_4^+ that results in a smaller number of water molecules in the first solvation shell compared to K^+. For the latter, the presence of a larger number of water molecules in the solvation shell introduces additional ion–water interactions that stabilize the ion solvation, leading to a slightly larger solvation energy than NH_4^+.

Finally, in the context of ion selectivity, a slightly smaller solvation energy of NH_4^+ compared to that of K^+ implies that NH_4^+ is easier to be desolvated and migrate into nanopores or ion-exchange membranes. However, it is important to emphasize that the activation energy for ion transport through, *e.g.*, membranes also depends on the chemistry of the membranes. For instance, it was shown in a recent study that although NH_4^+ exhibits a slightly smaller solvation energy, it experiences a higher activation energy compared to K^+ for ion permeation in ion-exchange membranes.[8] In this regards, additional interactions with membranes may play an important role due to the difference in the chemical composition between NH_4^+ and K^+, which will be the topic of future studies.

Conflicts of interest

There are no conflicts to declare.

Acknowledgements

This work was performed under the auspices of the U.S. Department of Energy by Lawrence Livermore National Laboratory under Contract DE-AC52-07NA27344. All the authors were supported as part of the Center for Enhanced Nanofluidic Transport, an Energy Frontier Research Center funded by the U.S. Department of Energy, Office of Science, Basic Energy Sciences under Award No. DE-SC0019112. Computational resources were from the Lawrence Livermore National Laboratory Institutional Computing Grand Challenge Program.

References

1 W. Deen, Hindered transport of large molecules in liquid-filled pores, *AIChE J.*, 1987, **33**, 1409–1425.
2 J. Schaep, B. Van der Bruggen, C. Vandecasteele and D. Wilms, Influence of ion size and charge in nanofiltration, *Sep. Purif. Technol.*, 1998, **14**, 155–162.
3 B. Van der Bruggen, A. Koninckx and C. Vandecasteele, Separation of monovalent and divalent ions from aqueous solution by electrodialysis and nanofiltration, *Water Res.*, 2004, **38**, 1347–1353.
4 M. A. Shannon; P. W. Bohn; M. Elimelech; J. G. Georgiadis; B. J. Marinas and A. M. Mayes, *Nanoscience and technology: a collection of reviews from nature Journals*, World Scientific, 2010, pp. 337–346.
5 M. Elimelech and W. A. Phillip, The future of seawater desalination: energy, technology, and the environment, *Science*, 2011, **333**, 712–717.
6 R. H. Tunuguntla, R. Y. Henley, Y.-C. Yao, T. A. Pham, M. Wanunu and A. Noy, Enhanced water permeability and tunable ion selectivity in subnanometer carbon nanotube porins, *Science*, 2017, **357**, 792–796.
7 R. Epsztein, E. Shaulsky, N. Dizge, D. M. Warsinger and M. Elimelech, Role of ionic charge density in donnan exclusion of monovalent anions by nanofiltration, *Environ. Sci. Technol.*, 2018, **52**, 4108–4116.
8 R. Epsztein, E. Shaulsky, M. Qin and M. Elimelech, Activation behavior for ion permeation in ion-exchange membranes: Role of ion dehydration in selective transport, *J. Membr. Sci.*, 2019, **580**, 316–326.
9 C. Song and B. Corry, Intrinsic ion selectivity of narrow hydrophobic pores, *J. Phys. Chem. B*, 2009, **113**, 7642–7649.
10 L. A. Richards, A. I. Schäfer, B. S. Richards and B. Corry, The importance of dehydration in determining ion transport in narrow pores, *Small*, 2012, **8**, 1701–1709.
11 O. Beckstein, K. Tai and M. S. Sansom, Not ions alone: barriers to ion permeation in nanopores and channels, *J. Am. Chem. Soc.*, 2004, **126**, 14694–14695.
12 O. Beckstein and M. S. Sansom, The influence of geometry, surface character, and flexibility on the permeation of ions and water through biological pores, *Phys. Biol.*, 2004, **1**, 42.
13 J. K. Holt, H. G. Park, Y. Wang, M. Stadermann, A. B. Artyukhin, C. P. Grigoropoulos, A. Noy and O. Bakajin, Fast mass transport through sub-2-nanometer carbon nanotubes, *Science*, 2006, **312**, 1034–1037.
14 B. Corry, Designing carbon nanotube membranes for efficient water desalination, *J. Phys. Chem. B*, 2008, **112**, 1427–1434.
15 F. Fornasiero, H. G. Park, J. K. Holt, M. Stadermann, C. P. Grigoropoulos, A. Noy and O. Bakajin, Ion exclusion by sub-2-nm carbon nanotube pores, *Proc. Natl. Acad. Sci. U. S. A.*, 2008, **105**, 17250–17255.
16 X. Gong, J. Li, K. Xu, J. Wang and H. Yang, A controllable molecular sieve for Na+ and K+ ions, *J. Am. Chem. Soc.*, 2010, **132**, 1873–1877.
17 B. Corry, Water and ion transport through functionalised carbon nanotubes: implications for desalination technology, *Energy Environ. Sci.*, 2011, **4**, 751–759.
18 L. A. Richards, B. S. Richards, B. Corry and A. I. Schafer, Experimental energy barriers to anions transporting through nanofiltration membranes, *Environ. Sci. Technol.*, 2013, **47**, 1968–1976.
19 S. A. Hawks, M. R. Cerón, D. I. Oyarzun, T. A. Pham, C. Zhan, C. K. Loeb, D. Mew, A. Deinhart, B. C. Wood and J. G. Santiago, *et al.*, Using Ultramicroporous Carbon for the Selective Removal of Nitrate with Capacitive Deionization, *Environ. Sci. Technol.*, 2019, **53**, 10863–10870.
20 S. Faucher, N. Aluru, M. Z. Bazant, D. Blankschtein, A. H. Brozena, J. Cumings, J. Pedro de Souza, M. Elimelech, R. Epsztein and J. T. Fourkas, *et al.*, Critical Knowledge

Gaps in Mass Transport through Single-Digit Nanopores: A Review and Perspective, *J. Phys. Chem. C*, 2019, **123**, 21309–21326.

21 P. Wingfield, Protein precipitation using ammonium sulfate, *Curr. Protoc. Protein Sci.*, 1998, **13**, A–3F.

22 D. N. Mortensen and E. R. Williams, Investigating protein folding and unfolding in electrospray nanodrops upon rapid mixing using theta-glass emitters, *Anal. Chem.*, 2014, **87**, 1281–1287.

23 A. Späth and B. König, Molecular recognition of organic ammonium ions in solution using synthetic receptors, *Beilstein J. Org. Chem.*, 2010, **6**, 32.

24 N. Widiastuti, H. Wu, H. M. Ang and D. Zhang, Removal of ammonium from greywater using natural zeolite, *Desalination*, 2011, **277**, 15–23.

25 H. A. Hasan, S. R. S. Abdullah, S. K. Kamarudin, N. T. Kofli and N. Anuar, Simultaneous NH4+-N and Mn2+ removal from drinking water using a biological aerated filter system: Effects of different aeration rates, *Sep. Purif. Technol.*, 2013, **118**, 547–556.

26 J. Huang, N. R. Kankanamge, C. Chow, D. T. Welsh, T. Li and P. R. Teasdale, Removing ammonium from water and wastewater using cost-effective adsorbents: A review, *Int. J. Environ. Sci.*, 2018, **63**, 174–197.

27 Y. Marcus, Effect of ions on the structure of water: structure making and breaking, *Chem. Rev.*, 2009, **109**, 1346–1370.

28 F. Gygi, Qbox, a Scalable Implementation of First-Principles Molecular Dynamics, http://eslab.ucdavis.edu.

29 J. P. Perdew, K. Burke and M. Ernzerhof, Generalized gradient approximation made simple, *Phys. Rev. Lett.*, 1996, **77**, 3865.

30 M. Schlipf and F. Gygi, Optimization algorithm for the generation of ONCV pseudopotentials, *Comput. Phys. Commun.*, 2015, **196**, 36–44.

31 T. A. Pham, T. Ogitsu, E. Y. Lau and E. Schwegler, Structure and dynamics of aqueous solutions from PBE-based first-principles molecular dynamics simulations, *J. Chem. Phys.*, 2016, **145**, 154501.

32 J. C. Grossman, E. Schwegler, E. W. Draeger, F. Gygi and G. Galli, Towards an assessment of the accuracy of density functional theory for first principles simulations of water, *J. Chem. Phys.*, 2004, **120**, 300–311.

33 E. Schwegler, J. C. Grossman, F. Gygi and G. Galli, Towards an assessment of the accuracy of density functional theory for first principles simulations of water. II., *J. Chem. Phys.*, 2004, **121**, 5400–5409.

34 G. Bussi, D. Donadio and M. Parrinello, Canonical sampling through velocity rescaling, *J. Chem. Phys.*, 2007, **126**, 014101.

35 C. Zhang, J. Wu, G. Galli and F. Gygi, Structural and vibrational properties of liquid water from van der Waals density functionals, *J. Chem. Theory Comput.*, 2011, **7**, 3054–3061.

36 R. A. DiStasio Jr, B. Santra, Z. Li, X. Wu and R. Car, The individual and collective effects of exact exchange and dispersion interactions on the ab initio structure of liquid water, *J. Chem. Phys.*, 2014, **141**, 084502.

37 O. Marsalek and T. E. Markland, Quantum dynamics and spectroscopy of ab initio liquid water: The interplay of nuclear and electronic quantum effects, *J. Phys. Chem. Lett.*, 2017, **8**, 1545–1551.

38 A. P. Gaiduk, C. Zhang, F. Gygi and G. Galli, Structural and electronic properties of aqueous NaCl solutions from ab initio molecular dynamics simulations with hybrid density functionals, *Chem. Phys. Lett.*, 2014, **604**, 89–96.

39 A. P. Gaiduk and G. Galli, Local and global effects of dissolved sodium chloride on the structure of water, *J. Phys. Chem. Lett.*, 2017, **8**, 1496–1502.

40 L. Zheng, M. Chen, Z. Sun, H.-Y. Ko, B. Santra, P. Dhuvad and X. Wu, Structural, electronic, and dynamical properties of liquid water by ab initio molecular dynamics based on SCAN functional within the canonical ensemble, *J. Chem. Phys.*, 2018, **148**, 164505.

41 M. D. LaCount and F. Gygi, Ensemble first-principles molecular dynamics simulations of water using the SCAN meta-GGA density functional, *J. Chem. Phys.*, 2019, **151**, 164101.

42 S.-Y. Ma, L.-M. Liu and S.-Q. Wang, Water film adsorbed on the α-Al_2O_3 (0001) surface: structural properties and dynamical behaviors from first-principles molecular dynamics simulations, *J. Phys. Chem. C*, 2016, **120**, 5398–5409.

43 T. A. Pham, S. G. Mortuza, B. C. Wood, E. Y. Lau, T. Ogitsu, S. F. Buchsbaum, Z. S. Siwy, F. Fornasiero and E. Schwegler, Salt Solutions in Carbon Nanotubes: The Role of Cation-π Interactions, *J. Phys. Chem. C*, 2016, **120**, 7332–7338.

44 G. Cassone, F. Creazzo, P. V. Giaquinta, F. Saija and A. M. Saitta, Ab initio molecular dynamics study of an aqueous NaCl solution under an electric field, *Phys. Chem. Chem. Phys.*, 2016, **18**, 23164–23173.

45 G. Cassone, F. Creazzo, P. V. Giaquinta, J. Sponer and F. Saija, Ionic diffusion and proton transfer in aqueous solutions of alkali metal salts, *Phys. Chem. Chem. Phys.*, 2017, **19**, 20420–20429.

46 T. A. Pham, Y. Ping and G. Galli, Modelling heterogeneous interfaces for solar water splitting, *Nat. Mater.*, 2017, **16**, 401.

47 T. A. Pham, M. Govoni, R. Seidel, S. E. Bradforth, E. Schwegler and G. Galli, Electronic structure of aqueous solutions: Bridging the gap between theory and experiments, *Sci. Adv.*, 2017, **3**, e1603210.

48 T. A. Pham, X. Zhang, B. C. Wood, D. Prendergast, S. Ptasinska and T. Ogitsu, Integrating Ab Initio Simulations and X-ray Photoelectron Spectroscopy: Toward A Realistic Description of Oxidized Solid/Liquid Interfaces, *J. Phys. Chem. Lett.*, 2017, **9**, 194–203.

49 K. J. Harmon, Y. Chen, E. J. Bylaska, J. G. Catalano, M. J. Bedzyk, J. H. Weare and P. Fenter, Insights on the Alumina–Water Interface Structure by Direct Comparison of Density Functional Simulations with X-ray Reflectivity, *J. Phys. Chem. C*, 2018, **122**, 26934–26944.

50 G. Cassone, D. Chillé, C. Foti, O. Giuffré, R. C. Ponterio, J. Sponer and F. Saija, Stability of hydrolytic arsenic species in aqueous solutions: As^{3+} *vs.* As^{5+}, *Phys. Chem. Chem. Phys.*, 2018, **20**, 23272–23280.

51 C. Zhang, D. Donadio, F. Gygi and G. Galli, First principles simulations of the infrared spectrum of liquid water using hybrid density functionals, *J. Chem. Theory Comput.*, 2011, **7**, 1443–1449.

52 A. P. Gaiduk, J. Gustafson, F. Gygi and G. Galli, First-principles simulations of liquid water using a dielectric-dependent hybrid functional, *J. Phys. Chem. Lett.*, 2018, **9**, 3068–3073.

53 W. Dawson and F. Gygi, Equilibration and analysis of first-principles molecular dynamics simulations of water, *J. Chem. Phys.*, 2018, **148**, 124501.

54 J. Carlsson and J. Åqvist, Absolute hydration entropies of alkali metal ions from molecular dynamics simulations, *J. Phys. Chem. B*, 2009, **113**, 10255–10260.

55 L. X. Dang, G. K. Schenter, V.-A. Glezakou and J. L. Fulton, Molecular Simulation Analysis and X-ray Absorption Measurement of Ca2+, K+ and Cl- Ions in Solution, *J. Phys. Chem. B*, 2006, **110**, 23644–23654.

56 T. T. Duignan, G. K. Schenter, J. L. Fulton, T. Huthwelker, M. Balasubramanian, M. Galib, M. D. Baer, J. Wilhelm, J. Hutter and M. Del Ben, *et al.*, Quantifying the hydration structure of sodium and potassium ions: taking additional steps on Jacob's Ladder, *Phys. Chem. Chem. Phys.*, 2020, DOI: 10.1039/C9CP06161D.

57 J. Sun, A. Ruzsinszky and J. P. Perdew, Strongly constrained and appropriately normed semilocal density functional, *Phys. Rev. Lett.*, 2015, **115**, 036402.

58 J. Sun, R. C. Remsing, Y. Zhang, Z. Sun, A. Ruzsinszky, H. Peng, Z. Yang, A. Paul, U. Waghmare and X. Wu, *et al.*, Accurate first-principles structures and energies of diversely bonded systems from an efficient density functional, *Nat. Chem.*, 2016, **8**, 831.

59 R. Mancinelli, A. Botti, F. Bruni, M. Ricci and A. Soper, Hydration of sodium, potassium, and chloride ions in solution and the concept of structure maker/breaker, *J. Phys. Chem. B*, 2007, **111**, 13570–13577.

60 F. Brugé, M. Bernasconi and M. Parrinello, Ab initio simulation of rotational dynamics of solvated ammonium ion in water, *J. Am. Chem. Soc.*, 1999, **121**, 10883–10888.

61 T.-M. Chang and L. X. Dang, On rotational dynamics of an NH^{4+} ion in water, *J. Chem. Phys.*, 2003, **118**, 8813–8820.

62 M. Ekimova, W. Quevedo, Ł. Szyc, M. Iannuzzi, P. Wernet, M. Odelius and E. T. Nibbering, Aqueous solvation of ammonia and ammonium: Probing hydrogen bond motifs with FT-IR and soft X-ray spectroscopy, *J. Am. Chem. Soc.*, 2017, **139**, 12773–12783.

63 Y. Marcus, Thermodynamics of solvation of ions. Part 5—Gibbs free energy of hydration at 298.15 K, *J. Chem. Soc., Faraday Trans.*, 1991, **87**, 2995–2999.

64 K. P. Jensen and W. L. Jorgensen, Halide, ammonium, and alkali metal ion parameters for modeling aqueous solutions, *J. Chem. Theory Comput.*, 2006, **2**, 1499–1509.

65 G. Lamoureux and B. Roux, Absolute hydration free energy scale for alkali and halide ions established from simulations with a polarizable force field, *J. Phys. Chem. B*, 2006, **110**, 3308–3322.

66 X. Duan and I. Nakamura, A new lattice Monte Carlo simulation for dielectric saturation in ion-containing liquids, *Soft Matter*, 2015, **11**, 3566–3571.

67 L. Liu and I. Nakamura, Solvation Energy of Ions in Polymers: Effects of Chain Length and Connectivity on Saturated Dipoles near Ions, *J. Phys. Chem. B*, 2017, **121**, 3142–3150.

68 I. Nakamura, Effects of Dielectric Inhomogeneity and Electrostatic Correlation on the Solvation Energy of Ions in Liquids, *J. Phys. Chem. B*, 2018, **122**, 6064–6071.

69 I. Nakamura, A.-C. Shi and Z.-G. Wang, Ion solvation in liquid mixtures: Effects of solvent reorganization, *Phys. Rev. Lett.*, 2012, **109**, 257802.

